JOURNAL OF SPACECRAFT AND ROCKETS
Vol. 46, No. 5, September–October 2009

Electrostatic Discharge Test on the Cu (In, Ga) Se_2 Solar Cell Array

Teppei Okumura,* Kazuhiro Toyoda,† and Mengu Cho‡
Kyushu Institute of Technology, Kitakyushu 804-8550, Japan
and
Shirou Kawakita§ and Mitsuru Imaizumi¶
Japan Aerospace Exploration Agency, Tsukuba 305-8505, Japan

DOI: 10.2514/1.41673

The boundary part of dielectric material, conductive material, and space, known as the triple junction, causes electrostatic discharge. Because the triple junction does not exist on the Cu (In, Ga) Se_2 solar cell surface, it should be free of electrostatic discharge. Electrostatic discharge tests on Cu (In, Ga) Se_2 were performed in a vacuum chamber which simulated the plasma environment in low Earth orbit and the high-energy electron environment in geostationary orbit. Contrary to the theoretical expectations, electrostatic discharge occurred on the surface of Cu (In, Ga) Se_2 and Cu (In, Ga) Se_2 suffered degradation of electric performance. The arc track was investigated to make clear the degradation mechanism of Cu (In, Ga) Se_2. The arc track worked as a leak resistance because the *PN* junction collapsed and the materials of front and back surfaces electroded adhere along the arc track.

Nomenclature

C_{ext}	=	external capacitance, F
C_p	=	current waveform, A
dI_{leak}	=	differential of leak current, A
I_{leak}	=	leak current, A
$I_{\text{leak}_{\text{after}}}$	=	leak current after experiment, A
$I_{\text{leak}_{\text{before}}}$	=	leak current before experiment, A
I_{peak}	=	peak of primary arc current, A
N_{arc}	=	total number of arcs
N_{cis}	=	number of primary arcs at CIGS surface
N_{ele}	=	number of primary arca at electrode
P_{max}	=	maximum power of solar cell, W
$P_{\text{max}_{\text{after}}}$	=	maximum power after experiment, W
$P_{\text{max}_{\text{before}}}$	=	maximum power before experiment, W
P_{peak}	=	peak of primary arc power, W
Q_{arc}	=	charge of primary arc current, C
R_r	=	resistance, Ω
R_s	=	series resistance of solar cell, Ω
R_{sh}	=	parallel resistance of solar cell, Ω
T_{i1}	=	start time of primary arc current, s
T_{i2}	=	end time of primary arc current, s
T_{p1}	=	start time of primary arc power waveform, s
T_{p2}	=	end time of primary arc power waveform, s
V_b	=	bias voltage, V
V_p	=	voltage waveform, V
W_{arc}	=	energy of primary arc, J

Received 20 October 2008; revision received 14 May 2009; accepted for publication 2 June 2009.

*Postdoctoral Fellow, Department of Electric Engineering, Tobata-ku; okumura@ele.kyutech.ac.jp.

†Associate Professor, Laboratories of Spacecraft Environment Engineering, Tobata-ku; toyoda@ele.kyutech.ac.jp.

‡Professor, Department of Electrical Engineering, Tobata-ku; cho@ele.kyutech.ac.jp. Senior Member AIAA.

§Engineer, Spacecraft Power Systems Group, 2-1-1 Sengen Tsukuba; kawakita.shirou@jaxa.jp.

¶Associate Senior Engineer, Spacecraft Power Systems Group, 2-1-1 Sengen Tsukuba; imaizumi.mitsuru@jaxa.jp.

I. Introduction

A THIN-FILM solar cell, constructed of amorphous silicon or Cu (In, Ga) Se_2 (CIGS), is considered a promising candidate as a future space solar cell because of its low mass and high light conversion efficiency [1]. The efficiency of CIGS (12% at air mass 0) is greater than that of any other type of thin-film solar cell. Because it is possible to deposit the solar cell on a thin metal sheet and a polyimide sheet, the thin-film solar array provides greater mass reduction and higher storage efficiency than the currently used solar arrays [2].

To construct a CIGS solar array paddle, the durability of CIGS when exposed to space radiation and space plasma needs to be investigated in terms of degradation of electric performance. Through the flight investigation onboard the MDS-1 (Tsubasa) satellite, CIGS demonstrated high durability against space radiation [3]. However, discharge on solar array due to spacecraft charging has recently become a serious concern, as the solar cell can potentially suffer degradation of electrical performance [4,5].

The cross-sectional view of a solar array of conventional design is shown in Fig. 1. There is a so-called triple junction which is the boundary of dielectric, conductor, or semiconductor and space. When a substorm event occurs in the geostationary orbit (GEO), the spacecraft potential with respect to ambient plasma becomes several kilovolts due to the incoming high-energy electrons. The potential of the dielectric surface (such as cover glass) on the solar array becomes positive with regards to the spacecraft body because of the secondary electron emission. The potential gradient inside the dielectric is called the inverted potential gradient.

In low Earth orbit (LEO), the spacecraft charges due to ionospheric plasma. The spacecraft body has negative potential with respect to the ambient plasma because of the difference of mobility between ions and electrons. The potential of the dielectric part on the solar array becomes positive with respect to the spacecraft body due to ion collisions. Thus, an inverted potential gradient is generated in LEO inside the dielectric material in a similar way to the case in GEO.

The triple junction enhances the intensity of the electric field. Because of the electric field emission phenomena, the electrons are emitted by the conductor or semiconductor near the triple junction. This electron emission leads to the discharge [6], which is known as primary arc.

The cross-sectional view of CIGS is shown in Fig. 2. Although CIGS is deposited on the glass substrate, the conductive materials, such as CIGS, molybdenum, and ZnO, are exposed to space.

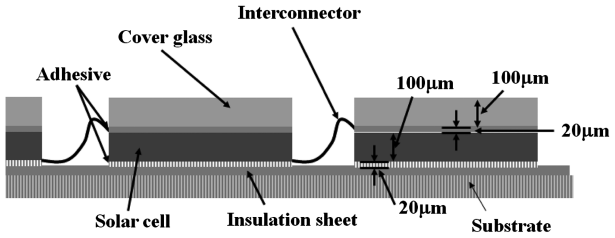

Fig. 1 Cross-sectional view of a solar array of conventional design.

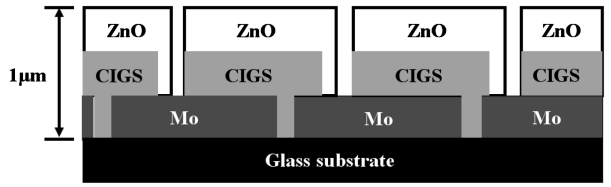

Fig. 2 Cross-sectional view of CIGS.

Therefore, because the triple junction does not exist on the surface, no primary arc is expected.

Galofaro et al. carried out an electrostatic discharge (ESD) experiment on various thin-film solar arrays including CIGS solar array and found CIGS solar array arced in a low temperature plasma environment simulating LEO plasma and suffered degradation of electrical performance [7]. The purpose of the present work is to investigate ESD on a CIGS solar cell further in detail. We performed ESD inception experiments on CIGS in a high-energy electron beam environment and in a plasma environment which simulated, respectively, the charging environment of GEO and LEO to investigate the primary arc inception. Section II describes the experiment in detail. We further performed an experiment to examine the solar cell degradation in the plasma environment. The degradation experiment is described in Sec. III along with a detailed analysis of the arc sites. In Sec. IV, we summarize the paper with suggestions of future work.

II. Electrostatic Discharge Inception Experiment

A. Experimental System

The waveform acquisition system consists of a high speed data acquisition board and a commercial PC (see Fig. 3). The system can measure the current and voltage waveform during the test. The high speed data acquisition board sends a trigger signal when the primary arc is detected. The peak, charge, and duration of the primary arc are simultaneously calculated. The image acquisition system identifies the primary arc position during the test. This system consists of an image acquisition board and a commercial PC. The video signal from a charge-coupled device (CCD) camera and the trigger signal from the waveform acquisition system are the inputs to the image acquisition board. Receiving the trigger signal, the system analyzes the video data to identify the primary arc position.

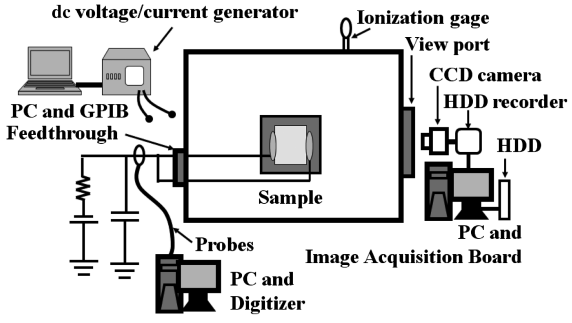

Fig. 3 Discharge experimental system, where HDD refers to the hard disk drive and GPIB refers to the general purpose interface bus.

B. Discharge Circuit

A discharge circuit as shown in Fig. 4 is employed in the concerned research institutes of France, USA, and Japan [8–10]. A voltage power supply V_b simulates the spacecraft potential with respect to the ambient plasma. A capacitance C_{ext} simulates the capacitance of the solar array. C_p supplies the primary arc current.

C. Electrostatic Discharge Inception Experiment in High-Energy Electron Beam Environment

The vacuum chamber which simulates the high-energy electron beam environment of GEO (GEO chamber) is equipped with an electron gun. The size of the GEO chamber is 0.6 m in diameter and 0.9 m in length. The acceleration voltage of the electron beam is 8 kV with current of 100 μA. The pressure is 6.2×10^{-4} Pa.

A CIGS sample, called a "large coupon," is shown in Fig. 5. The size of the large coupon is $100 \times 200 \times 5$ mm. Twenty-four CIGS are connected in series on the large coupon.

In the charging experiment in the GEO chamber, C_{ext} is 5.2 nF, V_b is -6 kV, and R_r is 10 MΩ. To measure the potential change on the CIGS surface before and after experiment, an electrostatic volt meter is used. The primary arc current is measured by using a current probe C_p (dc to 50 MHz). The voltage waveform is measured by using a high voltage probe V_p (dc to 25 MHz).

The large coupon was irradiated with an electron beam for 5 min. The potential difference is shown in Fig. 6. Because the surface potential does not change due to electron irradiation, CIGS does not charge due to the high-energy electrons.

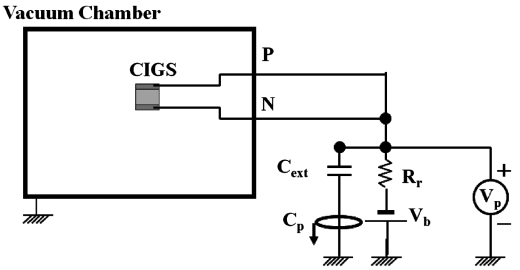

Fig. 4 Discharge circuit.

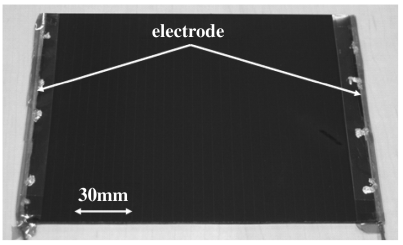

Fig. 5 CIGS large coupon.

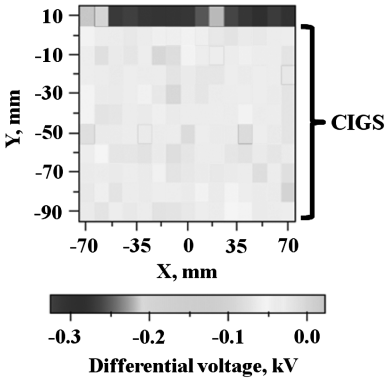

Fig. 6 Differential surface voltage on CIGS surface after 5-min electron irradiation.

A primary arc occurred after 16 min of beam irradiation even though the inverted potential gradient is not generated in the CIGS. A flash of the primary arc is shown in Fig. 7. The primary arc current waveform is shown in Fig. 8. Usually the primary arc current does not oscillate; however, the waveform shown in Fig. 8 oscillates more than 6 A to negative and positive directions. The primary arc occurs at the cable which is connected to the P electrode, instead of at the CIGS surface. The cable is thus charged due to high-energy electrons. The open circuit voltage of CIGS is 0.26 V after the experiment. Because the open circuit voltage before the experiment is 6.87 V, almost all of the CIGS on the large coupon suffer degradation in electric performance. Although the primary arc does not occur on the CIGS surface, the primary arc current flows through the CIGS (see Fig. 9). CIGS thus suffers degradation due to the primary arc current.

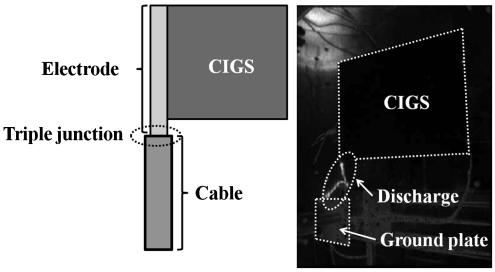

Fig. 7 Discharge at connector of CIGS large coupon.

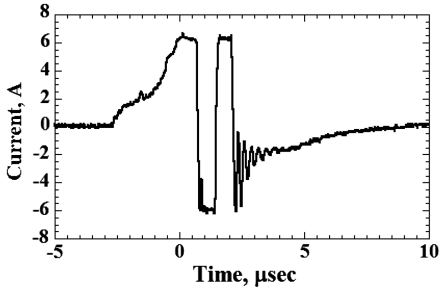

Fig. 8 Discharge current on CIGS large coupon. Note that the waveform is over the oscilloscope range beyond ±6 A.

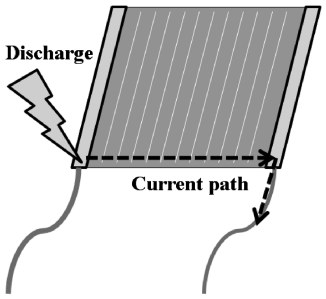

Fig. 9 Discharge current path.

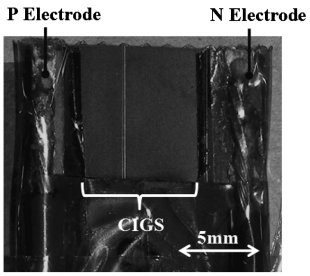

Fig. 10 CIGS small coupon.

Table 1 Experimental condition

	Large coupon	Small coupon
Pressure, Pa	3×10^{-2}	4×10^{-3}
Gas flow rate, sccm	0.3	0.4
Plasma density, m^3	1×10^{12}	1×10^{12}
Electron temperature, eV	1.0	1.0

D. Electrostatic Discharge Inception Experiment in Plasma Environment

The large coupon shown in Fig. 5 and the small coupon shown in Fig. 10 are used in the plasma environment. The small coupon was made to easily examine the surface on CIGS where the primary arc occurs. The size of the substrate of the small coupon is $10 \times 20 \times 5$ mm. One CIGS is deposited on the small coupon. To prevent a primary arc from forming, the electrodes are insulated by polyimide tape.

A vacuum chamber (LEO chamber) which simulates the plasma environment is equipped with an electron cyclotron resonance (ECR) plasma source. The size of the LEO chamber is 1.2 m in length and 1 m in diameter. Table 1 shows the experimental conditions for the small coupon and large coupon experiment. Although the pressure is different in the experiments for the small coupon and the large coupon, the ECR plasma source produced the same condition (plasma density and electron temperature) for the Xe plasma.

In the experiment with the large coupon, an inductance (270 μH) and a resistance (4Ω) are connected to the C_{ext} (5 μF) to simulate the primary arc current waveform. On the other hand, in the experiment with the small coupon, to avoid the degradation of CIGS due to the primary arc, C_{ext} is 540 pF without a resistance and inductance.

To investigate the primary arc inception voltage, we changed V_b from -100 V to -800 V. We started from a less negative value (-100 V) to more negative values. We defined the primary arc inception voltage as the voltage at which a primary arc occurs in each CIGS. Once the primary arc occurs on CIGS, the CIGS does not change the higher voltage bias. The maximum bias time is 90 min for a condition of V_b. In LEO, the day time is approximately 90 min; therefore, the maximum bias time is set to 90 min.

Table 2 shows the result of the ESD inception experiment in the plasma environment. "0" in Table 2 indicates the case when the primary arc does not occur even when the small coupon is biased. "——" in Table 2 indicates the case when the small coupon is not biased to avoid the degradation of CIGS due to repetitive primary arcs. The time is shown for such a condition. The minimum primary arc inception voltage is -200 V, although there are differences between each small coupon. The minimum primary arc inception voltage of the large coupon is also -200 V. Normally, the primary arc inception voltage on the InGaP/GaAs/Ge solar cell and the silicon solar cell is recognized to be approximately 200 V [11]. Therefore, the primary arc inception voltage of CIGS is at the same level as a solar cell actually used in the plasma environment.

The pressure is different for the experiments with the large coupon and the small coupon as shown in Table 1. Although it is supposed that the pressure affects primary arc frequency and inception voltage, no difference in primary arc inception voltage is seen. Normally, the primary arc frequency increases with the increase of V_b [11,12], however, in our experiment this was not observed.

The primary arc in the large coupon is shown in Fig. 11. The primary arc occurs on the surface of CIGS. We examined the surface of CIGS using a microscope before and after the experiment. However, we could not find the specific cause for the primary arc, such as a hole or tiny dust particles. The light intensity of the primary arc in the experiment with the small coupon is too weak to be detected.

III. Degradation Test

The primary arc occurs on the surface of CIGS in the charging experiment in plasma environment. We thereafter performed the degradation test on CIGS. The small coupon, shown in Fig. 10, was

Table 2 Result of ESD inception experiment under plasma environment

V_b	−200 V	−300 V	−400 V	−500 V	600 V	700 V	800 V
Large coupon	2	1	0	1	0	0	0
Small 1	0	0	2	——	——	——	——
Small 2	0	2	——	——	——	——	——
Small 3	0	0	0	1: 5 min	——	——	——
Small 4	0	1	——	——	——	——	——
Small 5	14: 65 min	——	——	——	——	——	——
Small 6	0	1	——	——	——	——	——
Small 7	4: 65 min	——	——	——	——	——	——

used. We focused on the condition of degradation and the degradation mechanism.

We used seven small coupons for the degradation test. The discharge circuit is as shown in Fig. 4. To vary the primary arc energy, we changed C_{ext} from 2 to 200 nF.

To check the degradation of CIGS due to the primary arc, we measured dark current-voltage characteristics (dark IV) after several primary arcs by using a source meter. Figure 12 shows the typical dark IV of CIGS. To examine the change of dark IV during the degradation test, we defined the current at 0.3 V as I_{leak}. Figure 13 shows an equivalent circuit of CIGS in a dark condition. R_{sh} is the parallel resistance, and R_s is series resistance.

The equivalent circuit of Fig. 13 is applied to the solar cell which has one *P-N* junction. Okumura et al. investigated the degradation of the silicon solar cell due to the primary arc [5]. In his experiment, it was found that I_{leak} of the silicon solar cell gradually increases after each primary arc incidence. This is because the parallel resistance of the silicon solar cell gradually decreases after each primary arc [5].

To examine the change of the solar cell performance before and after the degradation test, we used a solar simulator to measure the light current-voltage characteristic. Figure 14 shows the light power-voltage characteristic (light PV) of the small coupon. The maximum generation power is defined as $P_{\max}$.

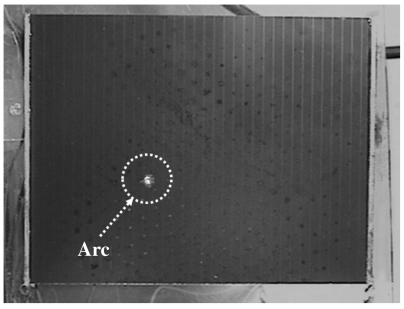

Fig. 11 Primary arc on large coupon.

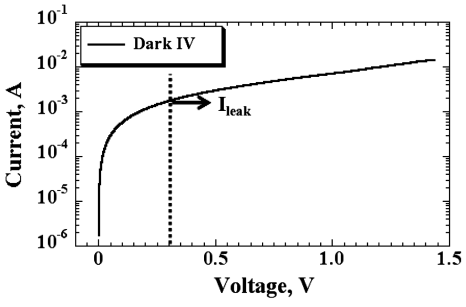

Fig. 12 Dark current-voltage characteristics of CIGS.

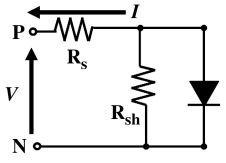

Fig. 13 Equivalent circuit of CIGS in dark condition.

A. Definition of Primary Arc Parameters

Figure 15 shows the typical primary arc voltage and current waveforms. The peak of the primary arc current is defined as I_{peak}. We defined T_{i1}, T_{i2} as the time when the current becomes 5% of I_{peak}. The charge of the primary arc Q_{arc} is defined as

$$Q_{\text{arc}} = \int_{T_{i1}}^{T_{i2}} i(t)\mathrm{d}t \tag{1}$$

The duration of primary arc T_{arc} is defined as

$$T_{\text{arc}} = T_{i2} - T_{i1} \tag{2}$$

To calculate the energy of the primary arc, we multiplied the voltage waveform by the current waveform to obtain the power waveform. Figure 16 shows the power waveform of the primary arc. The peak of the power waveform is defined as P_{peak}. We defined T_{p1}, T_{p2} as the time when the current becomes 5% of P_{peak}. The energy of primary arc W_{arc} is defined as

$$W_{\text{arc}} = \int_{T_{p1}}^{T_{p2}} i(t) \cdot v(t)\,\mathrm{d}t \tag{3}$$

B. Degradation of CIGS

Table 3 shows the results of the degradation test. It shows the condition of the degradation test, the primary arc parameters (I_{peak},

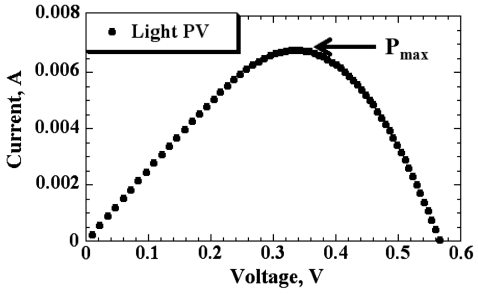

Fig. 14 Light power-voltage (PV) characteristics of small coupon.

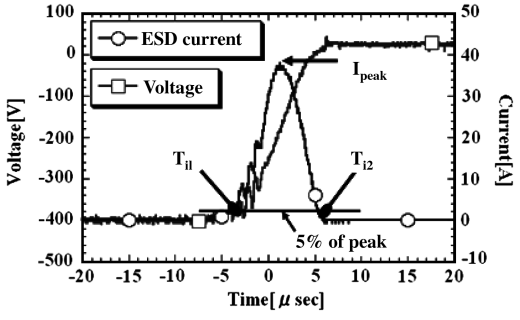

Fig. 15 Primary arc current and voltage waveform.

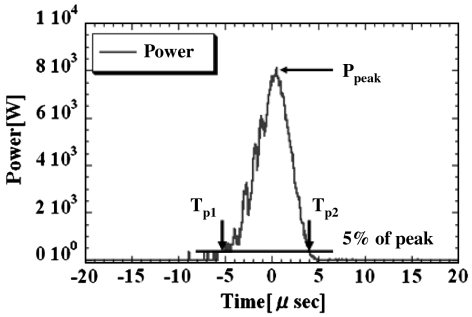

Fig. 16 Power waveform of primary arc.

T_{arc}, Q_{arc}, and W_{arc}), I_{leak} before and after experiment, and P_{max} before and after experiment. N_{cis} is the number of primary arcs which occur on the surface of CIGS. N_{ele} is the number of primary arcs which occur at the electrode. V_b is bias voltage. In the degradation test, we changed C_{ext} from 2 to 200 nF. To control the primary arc frequency, we changed V_b to an appropriate value.

W_{arc} was changed from 0.3 mJ minimum to 48 mJ maximum by varying C_{ext}. The minimum energy in the discharge experiment is much larger than that in the charging experiment discussed in Sec. II.D. Therefore, it was possible to detect the flash of the primary arc.

In Table 3, the bold characters used for W_{arc}, $I_{leak_{before}}$ and $I_{leak_{after}}$ values indicate the minimum condition in terms of W_{arc} where the small coupon suffers degradation. In the experiment for C05, C06, and C07, P_{max} decreases with increase of I_{leak}. In the cases of C05, C06, and C07, I_{leak} after the experiment is, respectively, 1.6, 24, and 130 times greater than I_{leak} before the experiment. On the contrary, the decrease rate of P_{max} is 38% in the case of C05, 64% in the case of C06, and 82% in the case of C07. So, a greater increase of I_{leak} leads to a greater decrease of P_{max}. This tendency is seen on another small coupon.

The primary arc parameter is minimum ($I_{peak} = 0.2$ A, $W_{arc} = 0.3$ mJ) in the case of C05 (2 nF). In this case, because I_{leak} increased after the experiment, C05 suffers degradation. The threshold energy for the degradation on the silicon solar cell was 30 mJ, and the threshold energy for the degradation on the InGaP/GaAs/Ge solar cell was about 3 mJ [9]. Therefore, CIGS is vulnerable against the primary arc compared with a traditional solar cell. The primary arc parameter is maximum ($I_{peak} = 31.6$ A, $W_{arc} = 48.0$ mJ) in the case of C04 (200 nF). In this case, as I_{leak} increased after the experiment, C04 suffers degradation. In the case of C04 (50 nF), although the primary arc parameter is larger than for C05 (2nF), I_{leak} does not increase after the experiment. This suggests that the primary arc on the surface of CIGS does not always cause degradation. In the cases of C01 (10 nF), C01 (50 nF), and C02 (50 nF), although the primary arc occurs on the surface of CIGS, I_{leak} recovers up to 13% of the maximum. The measurement error of dark IV is 3%; the reason why I_{leak} recovers for more than 3% is unknown.

We focused on the energy of the primary arc to understand the degradation in orbit. The primary arc generates the arc plasma which propagates on the solar array with a certain velocity. The arc plasma couples with the charged insulator on the arc plasma propagation area. The electrostatic discharge on the insulator is thus supplied to the primary arc. In GEO, the arc energy is supplied from the cover glass from an area of at least 1.4×0.6 m [12]. We assume the insulator, whose thickness is 100 μm and relative permittivity 2, has an inverted potential gradient of 100 V. 1 m^2 of the insulator supplies 0.9 mJ of energy. Therefore, an energy of 0.3 mJ is a possible value in real orbit.

Table 4 shows the details of the degradation test on C06. "Location" indicates the location of the primary arc on the small coupon. "Ele" refers to the primary arc that occurs on the electrode.

Table 3 Experimental result

Sample	C_{ext}, n	N_{arc}		I_{peak}, A	T_{arc}, μs	Q_{arc}, μC	W_{arc}, mJ	V_{min}, V	$I_{leak_{before}}$, mA	$I_{leak_{after}}$, mA	$P_{max_{before}}$	$P_{max_{after}}$
		N_{cis}	N_{ele}									
C01	5	2	2	0.3	18.9	3.69	**1.8**	−852	**4.32**	**7.62**	7.2	——
	10	3	0	1.0	20.9	8.86	4.0	−879	7.62	6.6	——	——
	50	3	0	4.8	27.5	50.6	25.0	−966	6.6	5.99	——	5.5
C02	5	3	0	0.2	18.8	2.87	0.9	−585	0.32	0.33	6.7	——
	10	3	0	0.6	22.4	5.65	1.7	−582	0.33	0.33	——	——
	50	9	0	3.0	27.7	32.1	10.0	−629	0.33	0.31	——	——
	100	5	4	5.4	41.6	67.0	**25.0**	−735	**0.31**	**7.5**	——	2.0
C03	5	3	0	0.3	17.6	3.33	1.2	−681	0.18	0.19	5.6	——
	10	3	0	0.8	24.4	9.09	**4.3**	−911	**0.19**	**10.0**	——	——
	50	2	0	4.2	31.8	50.1	25.0	−979	10.0	14.7	——	2.2
C04	10	5	3	0.4	24.1	5.08	1.7	−586	0.09	0.1	6.8	——
	50	4	1	2.2	33.8	26.3	8.3	−585	0.1	0.1	——	——
	100	9	4	5.3	32.9	59.2	**19.0**	−634	**0.1**	**2.93**	——	——
	200	5	0	10.4	31.6	137.0	48.0	−684	2.93	10.9	——	2.5
C05	2	48	4	0.2	12.5	1.04	**0.3**	−502	**1.66**	**2.77**	7.1	3.0
C06	5	6	3	0.3	12.7	2.47	**0.9**	−663	**0.62**	**14.9**	7.6	2.8
C07	10	13	20	0.5	20.0	5.48	**1.7**	−586	**0.15**	**19.6**	7.4	1.7

Table 4 Experimental result of C06

ID	I_{peak}, A	T_{arc}, μs	Q_{arc}, μC	W_{arc}, mJ	V_{min}, V	I_{leak}, mA	dI_{leak}, mA	Location
——	——	——	——	——	——	0.62	——	——
1	0.17	3.6	0.36	0.2	−592	——	——	Ele
2	0.18	3.8	0.4	0.22	−586	——	——	Ele
3	0.29	11.4	2.31	1.08	−683	——	——	Ele
4	0.32	16.4	3.16	1.17	−683	6.67	6.06	Cis
5	0.31	16.7	3.25	1.17	−683	8.94	2.27	Kap
6	0.27	18.5	3.24	1.17	−683	10.5	1.56	Kap
7	0.31	16.0	3.23	1.18	−683	12.3	1.8	Kap
8	0.28	14.8	3.14	1.17	−683	13.9	1.6	Kap
9	0.43	13.2	3.19	1.19	−683	14.9	1.0	Kap

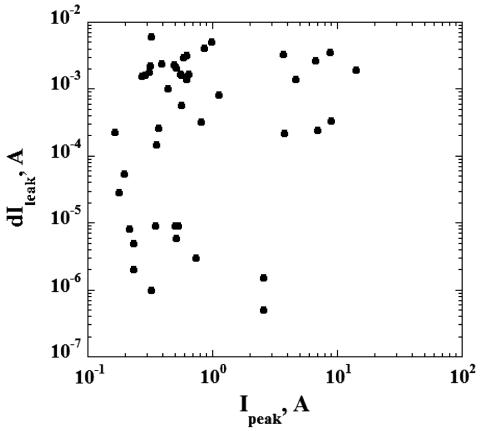

Fig. 17 Relationship between I_{peak} and dI_{leak}.

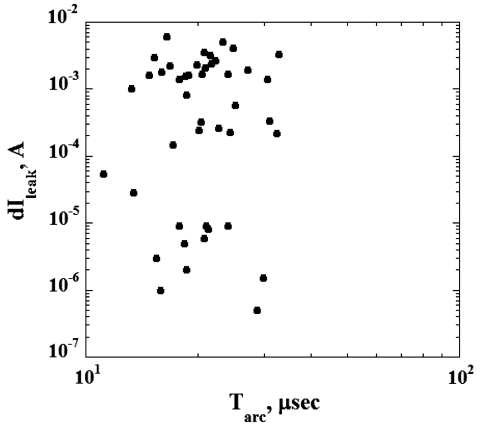

Fig. 18 Relationship between T_{arc} and dI_{leak}.

"Cis" points to the primary arc that occurs on the surface of CIGS. "Kap" refers to the primary arc that occurs at the boundary of CIGS and polyimide tape. The increase of I_{leak} in the case when the primary arc occurs on the surface of CIGS is defined as

$$\mathrm{d}I_{leak} = \frac{I_{after} - I_{before}}{N_{cis}} \tag{4}$$

Here, note that the number of primary arc at kap is included in N_{cis}. In the degradation test on C06, it was possible to measure the dark IV after each primary arc on the surface of CIGS. However, in the degradation test on the other small coupons, several primary arcs (19 primary arcs being maximum), occurred between the measurements of dark IV. Therefore, dI_{leak} indicates the average value of the increase of I_{leak} due to one primary arc occurring on the surface of CIGS.

"ID" denotes the primary arc number. It is seen from Table 4 that I_{leak} is increased after each primary arc on the surface of CIGS. This fact suggests that the electric performance of CIGS is gradually degraded due to repetitive primary arcs.

Figures 17–19 show the relation between I_{peak} and dI_{leak}, W_{arc} and dI_{leak}, and W_{arc} and dI_{leak}, respectively. It is difficult to find the obvious relationship between dI_{leak} and the arc parameters. In a series of degradation tests, the minimum arc parameter was found to be in the experimental condition of C05; I_{peak} being 0.2 A, T_{arc} being 12.5 μs, and W_{arc} being 0.3 mJ. Some of the small coupons did not suffer degradation even when W_{arc} is comparatively large, such as in the case of C04 (50 nF). However, there was no small coupon that survived unaffected at 25 mJ energy.

C. Degradation Mechanism of CIGS

It is recognized that the arc track created due to the primary arc works as a low parallel resistance of the solar cell [5]. It is thus

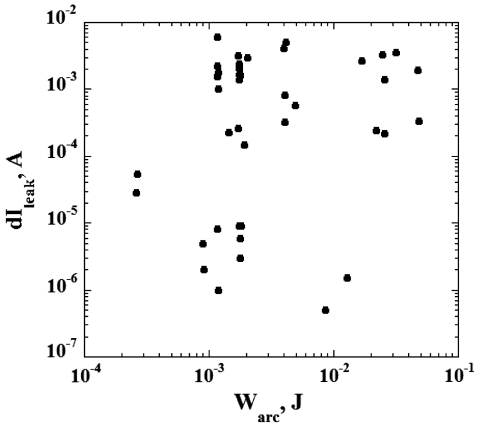

Fig. 19 Relationship between W_{arc} and dI_{leak}.

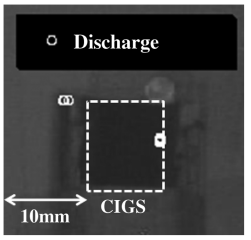

Fig. 20 Discharge position: C06.

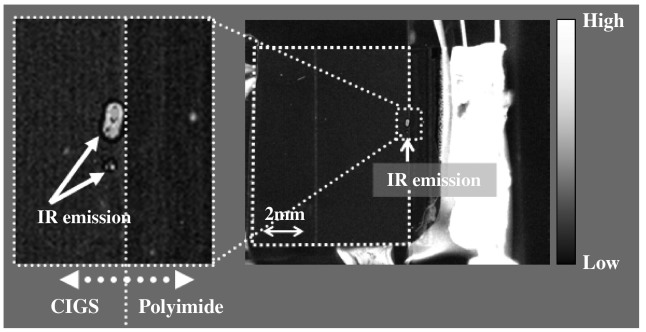

Fig. 21 IR emission on inverted bias: C06.

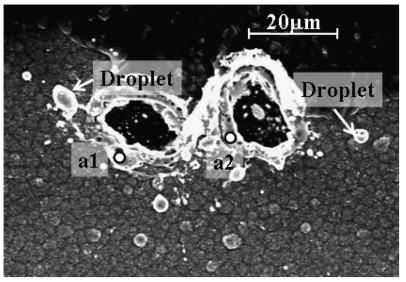

Fig. 22 SEM image of arc track on C06.

Table 5 Material composition at arc track

	a1	a2	CIGS	Droplet
Zn	49	50	84	62
O	8	9	16	13
In	20	11	——	8
Se	13	18	——	11
Mo	7	9	——	6
Si	3	3	——	——

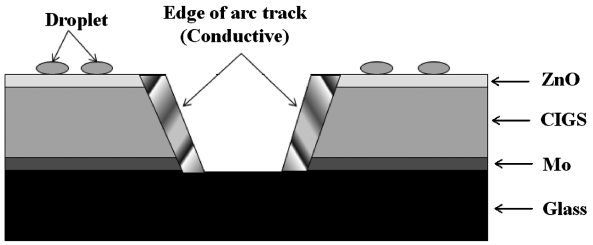

Fig. 23 Cross-sectional view of CIGS with arc track.

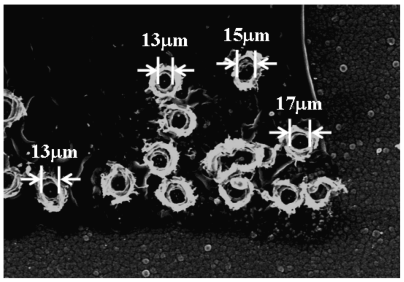

Fig. 24 Arc track on C05.

possible to detect infrared (IR) emission due to Joule heat because the current concentrates at the arc track. We investigated the current leak at the arc track using a photoemission microscope. The detector of the photoemission microscope is an InGaAs CCD camera, and it is able to detect maximum 1.7 μm of IR emission. Figure 20 shows the primary arc position on C06. As mentioned in Sec. II.D, the electrodes are covered by polyimide tape to prevent primary arc inception. CIGS (C06) is exposed inside the white frame in Fig. 20. Figure 21 shows an IR image of C06 with inverted bias at 1 V and 0.2 A. The white frame in Fig. 21 corresponds to the white frame in Fig. 20. The IR emission is detected where the primary arcs occur inside a red frame as in Fig. 21.

How does CIGS change due to a primary arc? Why does the arc track work as a parallel resistance? To answer these questions, we investigated the arc track by using a scanning electron microscope (SEM) and a surface analyzer. Figure 22 shows a SEM picture of the arc track on C06. There are a lot of droplets around the arc track. We analyzed the material composition at "a1" and "a2" by using a surface analyzer (see Table 5). The material composition where CIGS does not suffer degradation due to a primary arc is indicated by "CIGS." The material composition of the droplets is indicated by "droplet." In a part where the primary arc does not occur, Zn and O, the materials used in the transparent surface electrode, are detected. At the droplet, not only Zn and O but also In, Se, and Mo, the materials used in the CIGS and back surface electrode, are detected. Because the composition of the droplet is conductive, the droplet may not be a cause of the primary arc or the defective of CIGS. At the edge of the arc track, such as at a1 and a2, the transparent electrode material (ZnO), materials used for CIGS and the back surface electrode (Mo) are detected. Because the materials for surface electrode and back surface electrode are mixed at the edge of the arc track, the *P-N* junction collapses, and conductivity of the arc track is determined from the mixing rate of the conductive materials, such as Zn and Mo. Because the edge of the arc track is electrically coupled

Table 6 Material characteristics and melt energy of 4.4×10^{-16} m^3 of selenium, copper, and indium

	Molar volume, m^3/mol	Heat of fusion, kJ/mol	Melt energy per unit volume, J/m^3	Melt energy, J
Selenium	16.42×10^{-6}	6.69	4.1×10^{8}	1.8×10^{-7}
Copper	7.11×10^{-6}	13.05	1.8×10^{9}	8.1×10^{-7}
Indium	15.76×10^{-6}	3.26	2.1×10^{8}	9.1×10^{-8}

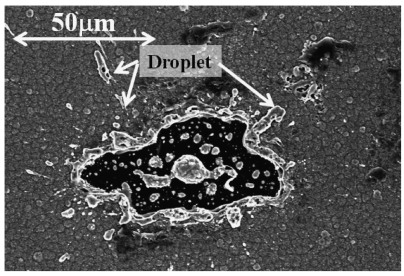

Fig. 25 Arc track not surrounded by an insulator.

with the surface electrode and the back surface electrode, the arc track works as a parallel resistance. Here, as a summary of the degradation mechanism, the cross-sectional view of CIGS with arc track is shown in Fig. 23.

We estimate the energy to melt the CIGS. Figure 24 shows the arc tracks on C05 (2 nF). The arc energy in the degradation test on C05 is small compared with other degradation tests. In Fig. 24, the maximum diameter of the arc track is 17 μm, and the minimum diameter is 13 μm. Because the thickness of CIGS is 2 μm, the maximum volume of the arc track is 4.4×10^{-16} m^3, and the minimum volume of the arc track is 2.5×10^{-16} m^3. Here, a typical CIGS consists of 49% of selenium, 24% of copper, 20% of indium, and 7% of gallium [1]. We estimate the energy to melt 4.4×10^{-16} m^3 of selenium, copper, and indium. Because the atomic mass of gallium is smaller than that of the other substances, we ignore gallium. Table 6 lists the molar volume, heat of fusion, and the energy to melt a volume of 4.4×10^{-16} m^3 [13]. Because the energy of the primary arc is 1.8×10^{-4} J in the degradation test on C05, the primary arc has enough energy to create the arc track.

D. Mechanism of the Primary Arc Inception

In the subsequent degradation test, most of the primary arcs occur at the places in connection with glass and polyimide tape. As the boundary of CIGS with the glass and polyimide tape is the triple junction, the primary arc can occur there. However, in some of the discharge tests in the plasma environment, such as in the cases of the large coupon and sometimes for the small coupon, the primary arc occurred on the surface of CIGS where there was no polyimide tape and glass adjacent. In the case of C02 (100 nF), a primary arc occurred on the surface of CIGS without the adjacent dielectric material; the arc track of this primary arc is shown in Fig. 25. From the result of the surface analysis around the arc track in Fig. 25, only the material for the surface electrode was detected. Therefore, the triple junction, which was the cause of the primary arc in Fig. 25, was not formed with polyimide sheet nor glass. It is possible that the triple junction was formed because of dust particles adhered to the surface before the experiment. Contamination can become the source of triple junction. Even in orbit, contamination may cause primary arcs on a CIGS surface. We plan to perform a laboratory experiment to prove this hypothesis in the near future.

IV. Conclusions

We performed the ESD tests on CIGS. From results of the experiment in a high-energy electron beam environment, it was found that CIGS did not charge due to an electron. This was because only the conductor or semiconductor was exposed on the surface. However, the primary arc occurred at a cable which was connected to CIGS, because the dielectric part of the cable charged due to the electrons. The primary arc had more than 6 A of peak current flowing into the large coupon for several microseconds, where 24 CIGS cells were connected in series. As a result, almost all of the CIGS cells degraded.

In the ESD test in a plasma environment, the primary arc occurred when the bias voltage became more than 200 V. The primary arc mostly occurred at the boundary of CIGS and insulator, such as glass and polyimide sheet. Therefore, the primary arc occurs as long as the triple junction exists on the CIGS surface either in GEO or LEO.

The degradation test was performed in a plasma environment. All CIGS suffered degradation in electric performance due to the primary arc. The cause of the degradation on CIGS was the arc track that worked as a leak resistance. From the result of surface analysis of the arc track, we found a mixture of the materials of the back surface electrode, the surface electrode, and CIGS which led to the collapse of the *PN* junction at the arc track. The minimum primary arc parameters for the degradation were 0.3 mJ energy, 0.2 A peak primary arc current, and 12.5 μs primary arc duration. None of the seven CIGS survived unaffected 25 mJ of energy. CIGS is more vulnerable against the primary arc compared with a traditional solar cell such as crystalline silicon or InGaP/GaAs/Ge. A primary arc with energy of 0.3 mJ is possible in an actual space environment. To realize a thin-film solar array, it is thus necessary to develop a primary arc mitigation technique.

We expected that the primary arc should not occur on the surface of CIGS, as the triple junction does not exist there. However, some of the primary arc occurred on the surface of CIGS. In the future, we have to further investigate the cause of the primary arc on the surface of CIGS to fully understand the primary arc inception mechanism.

Acknowledgments

We extend our appreciation to A. Owada, Y. Takeda, and M. Saito in the Advanced Engineering Service Co., Ltd., for their contributions to the discharge test.

References

[1] Hepp, A., McNatt, J., Dickman, J., Morel, D., Ferekides, C., Jin, M., Banger, K., Orbey, N., Cushman, M., Birkmire, R., and Shafarman, W., "Thin-Film Solar Cells on Polymer Substrates for Space Power," *2nd International Energy Conversion Engineering Conference on Disk* [CD-ROM], AIAA, Reston, VA, Aug. 2004; also AIAA Paper 2004-5737.

[2] Hausgen, P., Tlmok, P., Merrill, J., Granata, J., and Sneft, D., "AFRL Thin Film Solar Cell Development and Upcoming Flight Experiments," *2nd International Energy Conversion Engineering Conference on Disk* [CD-ROM], 2004-5734, AIAA, Reston, VA, Aug. 2004.

[3] Kawakita, S., Shimazaki, K., Imaizumi, M., Kuwajima, S., Yoda, Y., Ohshima, T., and Itoh, H., "Possibility Analysis of Cu(In, Ga) Se_2 Thin-Film Solar Cell for Space Use," *Proceedings of the 6th International Workshop on Radiation Effects on Semiconductor Devices for Space Application*, Japan Atomic Energy Agency, Takasaki, Gunma, Japan, 2004, pp. 151–154.

[4] Toyoda, K., Okumura, T., Hosoda, S., and Cho, M., "Degradation of High Voltage Solar Array Due to Arcing in LEO Plasma Environment," *Journal of Spacecraft and Rockets*, Vol. 42, No. 5, 2005, pp. 947–953. doi:10.2514/1.11602

[5] Okumura, T., Masui, H., Toyoda, K., Imaizumi, M., and Cho, M., "Degradation of Electric Performance due to Electrostatic Discharge on Silicon Solar Cell for Space," *Journal of the Japan Society for Aeronautical and Space Sciences*, Vol. 55, No. 647, 2007, pp. 590–596. doi:10.2322/jjsass.55.590

[6] Hastings, D., and Garrett, H., *Spacecraft Environment Interactions*, Cambridge Univ. Press, New York, 1996, pp. 142–198.

[7] Galofaro, J. T., Vayner, B. V., Hillard, B. G., and Ferguson, D. C., "SSTE-4 Program Advanced Photovoltaic Cell Technologies: Ground Chamber Test Results," *IEEE Transactions on Plasma Science* (to be published).

[8] Meteo-Velez, J-C., Inguimbert, V., Sarrail, D., Levy, L., Boulay, F., Roussel, J-F., Laffornt, E., and Payan, D., "Degradation of Solar Cell by ESDs," [CD-ROM] Centre National d'Etudes Spatiales, Toulouse, France, June 2007.

[9] Vayer, B., Furguson, D., and Galofaro, J., "Detrimental Effect of Arcing on Solar Array Surfaces," [CD-ROM] Centre National d'Etudes Spatiales, Toulouse, France, June 2007.

[10] Okumura, T., Ninomiya, S., Masui, H., Toyoda, K., Imaizumi, M., and Cho, M., "Solar Cell Degradation due to ESD for International Standardization of Solar Array ESD Test," [CD-ROM] Centre National d'Etudes Spatiales, Toulouse, France, June 2007.

[11] Hosoda, S., Okumura, T., Kim, J., Toyoda, K., and Cho, M., "Development of 400 V Solar Array Technology for Low Earth Orbit Plasma Environment," *IEEE Transactions on Plasma Science*, Vol. 34, No. 5, Oct. 2006, pp. 1986–1996. doi:10.1109/TPS.2006.883287

[12] Vayner, B., and Vayner, L., "Electrostatic Discharge on Triple Junction Solar Cells in Simulated LEO Environment," [CD-ROM] Centre National d'Etudes Spatiales, Toulouse, France, June 2007.

[13] Weast, R. C., Astle, M. J., and Beyer, W. H., *CRC Handbook of Chemistry and Physics: A Ready-Reference Book of Chemical and Physics Data*, 1st student ed., Chemical Rubber Company, Cleveland, OH, 1967.

A. Ketsdever
Associate Editor